Tomography and purification of the temporal-mode structure of quantum light
Supplemental Material

Vahid Ansari,[1] John M. Donohue,[1] Markus Allgaier,[1] Linda Sansoni,[1] Benjamin Brecht,[1,2]
Jonathan Roslund,[3] Nicolas Treps,[3] Georg Harder,[1] and Christine Silberhorn[1]

[1] *Integrated Quantum Optics, Paderborn University, Warburger Strasse 100, 33098 Paderborn, Germany*
[2] *Clarendon Laboratory, Department of Physics, University of Oxford, Parks Road, OX1 3PU, United Kingdom*
[3] *Laboratoire Kastler Brossel, UPMC-Sorbonne Universités, CNRS, ENS-PSL Research University, Collége de France; CC74, 4 Place Jussieu, 75252 Paris, France*

In this supplementary material, we provide technical details on the experimental setup, sketched in Fig. 1. In Table I, we provide measured parameters of the four PDC states explored in the main text, including the $g^{(2)}$ numbers displayed graphically in Fig. 3 of the main text. We also provide extra data detailing the purity of the PDC source as the PDC pump is chirped, as seen in Fig. 2. In Fig. 3, we provide both the real and imaginary parts of the reconstructed seven-dimensional density matrices, and compare their eigenvalues with the expected values from the JSI. In Fig. 4, we show the projections implemented by the QPG to reconstruct the seven-dimensional density matrices.

Our experiment is driven by an 80-MHz titanium-sapphire laser (Ti:Sa, Coherent Chameleon) and OPO (APE Compact). We create the PDC pump pulses at 769 nm by frequency doubling light from the OPO in 1 mm of bulk PPLN; the fundamental of the Ti:Sa at 876 nm is used as the QPG pump. Both pulses are shaped with approximately 0.05-nm resolution using a 4f setup consisting of a 2000 lines/mm diffracting grating, a curved mirror with a 250 mm focal length, and a reflective liquid-crystal spatial light modulator (SLM, Hamamatsu LCoS) at the focal plane [41, 42]. With this setup, we can directly control the bandwidth, spectral shape, and spectral phase of the pump pulses.

The PDC photons are generated through a near-degenerate type-II process in a 8-mm long PPKTP waveguide (AdvR) with a nominal poling period of 117 μm. An 80 nm broad bandpass filter is used to remove the PDC pump, and the individual photons are separated with a polarizing beamsplitter and filtered with 3 nm bandpass filters to remove side lobes. In all cases, the PDC pump energy was approximately 15 pJ per pulse, with heralded $g_h^{(2)}$s lying between 0.417 ± 0.003 for the spectrally decorrelated state and 0.246 ± 0.003 for the intensity-anticorrelated state. This

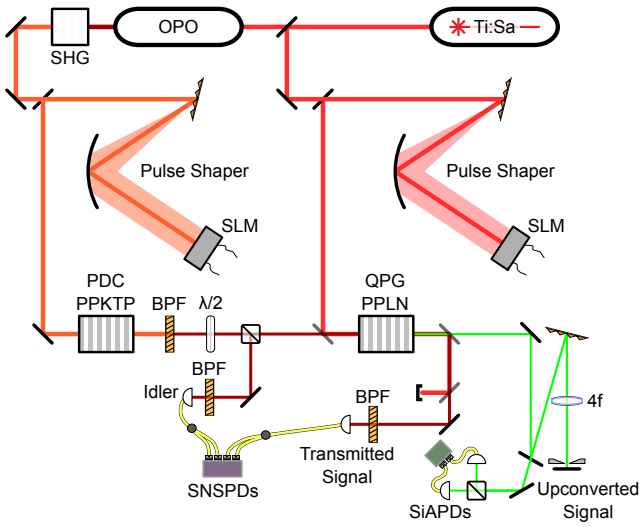

FIG. 1. **Experimental setup.** We create photon pairs through type-II PDC in an 8-mm PPKTP waveguide. By shaping the bandwidth and spectral phase of the PDC pump with a spatial light modulator (SLM) in a 4f line [41, 42], we can control the effective mode number of the generated photon pairs. The PDC pump is removed with a bandpass filter (BPF) and the photon pair is split with a polarizing beamsplitter (PBS). The signal photon is then coupled into a 17-mm PPLN waveguide acting as a quantum pulse gate (QPG), with a QPG pump shaped in both phase and amplitude by another SLM. A series of dichroic mirrors and a 4f line are used to split the upconverted and transmitted photons from the leftover QPG pump, and all photon paths are coupled into single-mode-fiber beamsplitters to measure second-order correlation functions.

relatively high production rate was used to enable reasonably precise unheralded $g^{(2)}$ measurements with 10-minute recording times. See Table I for all $g_h^{(2)}$ values. For ease of alignment, the signal photon path can be switched for a coherent pulse from the OPO, spectrally shaped by a commercial pulse shaper (Finisar WaveShaper 4000S). The average number of generated photons can be inferred from the two-photon cross-correlation statistics [40], with the average generation rate of $\langle n \rangle \approx 0.16$ for the decorrelated state deduced from a $g^{(1,1)} = \frac{1}{\langle n \rangle} + g^{(2)} = 8.303 \pm 0.003$.

The signal photons and the QPG pump (with an average energy-per-pulse of 250 pJ) are combined on a dichroic mirror and coupled into a 17-mm long PPLN waveguide with a poling period of 4.4 μm, fabricated in-house and designed for spatially single-mode propagation at 1540 nm. The waveguide mode of the QPG pump is imaged on a camera after the waveguide and optimized to the fundamental spatial mode. Higher-order modes produce sum-frequency signals for different time delays with central frequencies, and are filtered out of the final signal along with the second harmonic of the QPG pump by a 4f-filter. The upconverted light at 558 nm is measured on a spectrometer (Andor Shamrock SR500 spectrograph and Newton 970-BVF EMCCD camera with a 2398 lines/mm grating) to have a bandwidth of 61 pm FWHM. The 4f-filter is also used to remove spectral side lobes, which account for less than 5% of the total upconverted photons. The upconverted green photons were detected with silicon avalanche photodiodes (SiAPDs, Excelitas), while the idler and leftover signal photons were detected with superconducting nanowire single-photon detectors (SNSPDs, PhotonSpot). All three photon paths are split into two detectors to measure photon number correlations via Hanbury-Brown-Twiss interferometry [40].

The joint spectral intensities (JSIs) were measured with fiber-based time-of-flight spectrometers [43], mapping a spectral range of 1 nm at 1540 nm to a time delay of 0.42 ns. Assuming a flat spectral phase, the singular-value decomposition of the JSI predicts a spectral purity of 0.995 for the decorrelated JSI of Fig. 3a, and 0.652 for the intensity anticorrelated JSI of Fig. 3b. The marginal bandwidths (intensity FWHM) of the signal and idler photon in the decorrelated case were measured to be 4.9 nm and 3.6 nm, respectively.

To compensate for dispersive elements throughout the apparatus, the spectral phase of the PDC pump was optimized with the SLM to maximize the $g^{(2)}$ of the decorrelated state (Case 'a'), as seen in Fig. 2. The chirp of the phase-correlated PDC state of Fig. 3c is $A = 0.38 \times 10^6\,\mathrm{fs}^2$, where the chirp is represented as a phase in angular frequency as $\exp\left[iA(\omega - \omega_0)^2\right]$. Given a separable Gaussian PDC state with signal and idler bandwidths σ_s and σ_i (intensity standard deviation in ω), the expected purity as a function of pump chirp A is

$$P = \frac{1}{\sqrt{1 + 16A^2\sigma_s^2\sigma_i^2}}, \tag{1}$$

which is seen in Fig. 2 to match the experimental result well for large chirp values. While this result clearly shows that dispersion management of the pump is key for producing single-mode photons, it also provides an alternative avenue for generating highly entangled photon pair states. For tasks requiring highly multimode photons, this method of increasing the number of modes present can make use of the entire PDC pump bandwidth, and therefore does not significantly affect the pair generation rate of the source in power-limited situations.

The central wavelength and time delay of the QPG pump relative to the PDC signal photons were set by optimizing the ratio of upconversion between HG0 and HG1 projections. The spectral phase and bandwidth of the QPG pump were adjusted to maximize the visibility between HG0 and HG2 projections. Pulse bandwidths as measured on a spectrometer (Andor Shamrock SR500 with a 1200 l/mm grating) are given in Table I.

For the $g^{(2)}$ measurements of Fig. 4 of the main text, the QPG is effectively set to 'OFF' by delaying the pump by 5 ps, where it does not interact with the PDC photons. The QPG pump is delayed rather than blocked in order to ensure all three measurements are subject to the same background noise, which may arise from scattering of the transmitted QPG pump or a broadband parametric noise from errors in periodic poling [44]. With all laser pulses blocked, the ambient and detector dark-count rate was approximately 1.8k-per-detector-per-second for the SNSPDs and 350-per-detector-per-second for the APDs. Coincidences are registered within a 3 ns window, and the expected dark counts outside this window are subtracted. When the PDC pump is blocked but the QPG pump is coupled through the system, we measure extra background counts of approximately 4.9k and 80 counts-per-detector-per-second on the SNSPDs and APDs, respectively. This has a negligible effect on the measurements of the upconverted photons, but significantly impacts the $g^{(2)}$ of the transmitted PDC signal photons, as seen by comparing the "QPG pump blocked" and the "QPG pump delayed" $g^{(2)}$ values in Table I. Note that no background subtraction is employed for the tomography results, but they are conditioned upon coincidence with an idler detection. When measuring in coincidence, the background rate measured by the APDs drops below 8-per-detector-per-second, while the coincidence detection rate for the Gaussian projection onto the single-mode state is over 7000-per-detector-per-second, providing a more-than-satisfactory signal-to-noise.

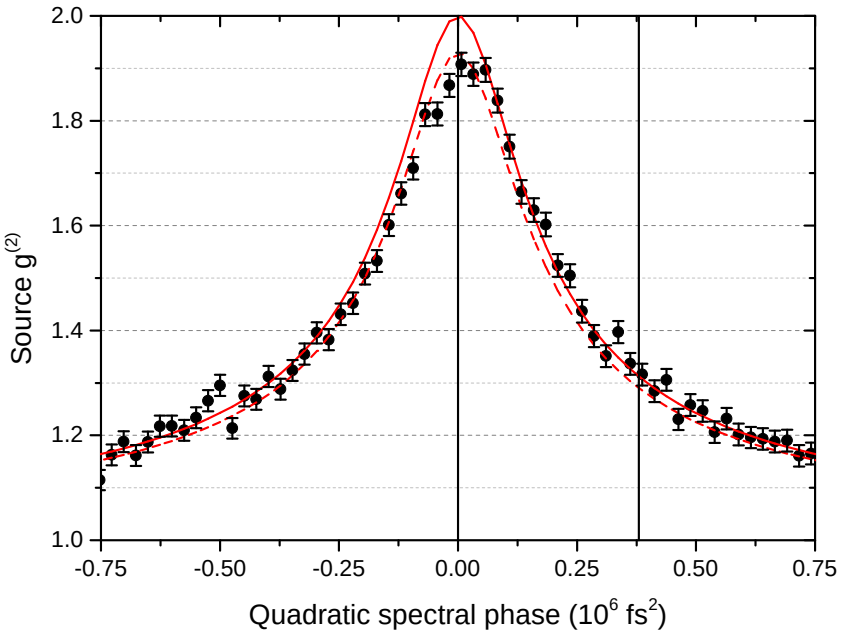

FIG. 2. **PDC source purity as spectral phase added.** The purity of the PDC source, as measured from the marginal $g^{(2)}$ of the signal photon with the QPG off, as a function of quadratic spectral phase of the form $e^{iA(\omega-\omega_0)^2}$ on the PDC pump. Five seconds of data were taken per spectral phase setting. The thick black lines represent the chirp values used for a high-purity PDC state (Case 'a') and a highly multimode PDC state (Case 'c'). The solid red curve is the theoretical expectation of Eq. 1, and the dashed red curve is the same curve with Poissonian background equivalent to 4% of the total count rate added to match the peak $g^{(2)}$ of 1.929 measured in the experiment.

Reference	(a)	(b)	(c)	(d)
PDC Pump Shape	HG0	HG0	HG0	HG1
PDC Pump Bandwidth	1.72 nm	0.54 nm	1.49 nm	1.31 nm
PDC Pump Chirp	0	0	0.38×10^6 fs^2	0
QPG Pump Bandwidth	1.54 nm	1.05 nm	1.58 nm	1.30 nm
Purity of ρ from reconstruction	0.896 ± 0.006	0.523 ± 0.008	0.317 ± 0.005	0.531 ± 0.004
Expected purity from JSI	0.995	0.652	0.377*	0.542*
Transmitted $g^{(2)}$, QPG pump blocked	1.929 ± 0.008	1.528 ± 0.010	1.327 ± 0.005	1.498 ± 0.006
Transmitted $g^{(2)}$, QPG pump delayed	1.861 ± 0.003	1.494 ± 0.003	1.302 ± 0.002	1.461 ± 0.003
Transmitted $g^{(2)}$, QPG pump HG0	1.827 ± 0.004	1.456 ± 0.004	1.277 ± 0.002	1.467 ± 0.003
Transmitted $g^{(2)}$, QPG pump HG1	1.875 ± 0.003	1.512 ± 0.004	1.308 ± 0.002	1.446 ± 0.003
Upconverted $g^{(2)}$, QPG pump HG0	1.975 ± 0.015	2.044 ± 0.037	1.983 ± 0.026	1.949 ± 0.033
Upconverted $g^{(2)}$, QPG pump HG1	2.078 ± 0.194	1.951 ± 0.105	1.925 ± 0.063	1.993 ± 0.025
Transmitted $g_h^{(2)}$, QPG pump delayed	0.417 ± 0.003	0.246 ± 0.003	0.374 ± 0.002	0.393 ± 0.003
Upconverted $g_h^{(2)}$, QPG pump HG0	0.423 ± 0.005	0.319 ± 0.009	0.501 ± 0.011	0.572 ± 0.017

TABLE I. Pump bandwidths and measured $g^{(2)}$s for the four PDC states explored in the main text, corresponding to the JSIs of Fig. 3. The error of the purity from the tomographically reconstructed density matrices ρ are found through Monte Carlo simulation assuming the coincidences measured have Poissonian error. The expected purity from the JSIs correspond to the singular value decomposition assuming a flat phase, except in cases marked (*) where faithful implementation of the intended phase is assumed. All $g^{(2)}$ values are corrected for detector dark counts assuming a 3 ns coincidence window. $g_h^{(2)}$ is the heralded second-order correlation function, which is zero for the ideal single-photon Fock state and one or greater for all classical states of light.

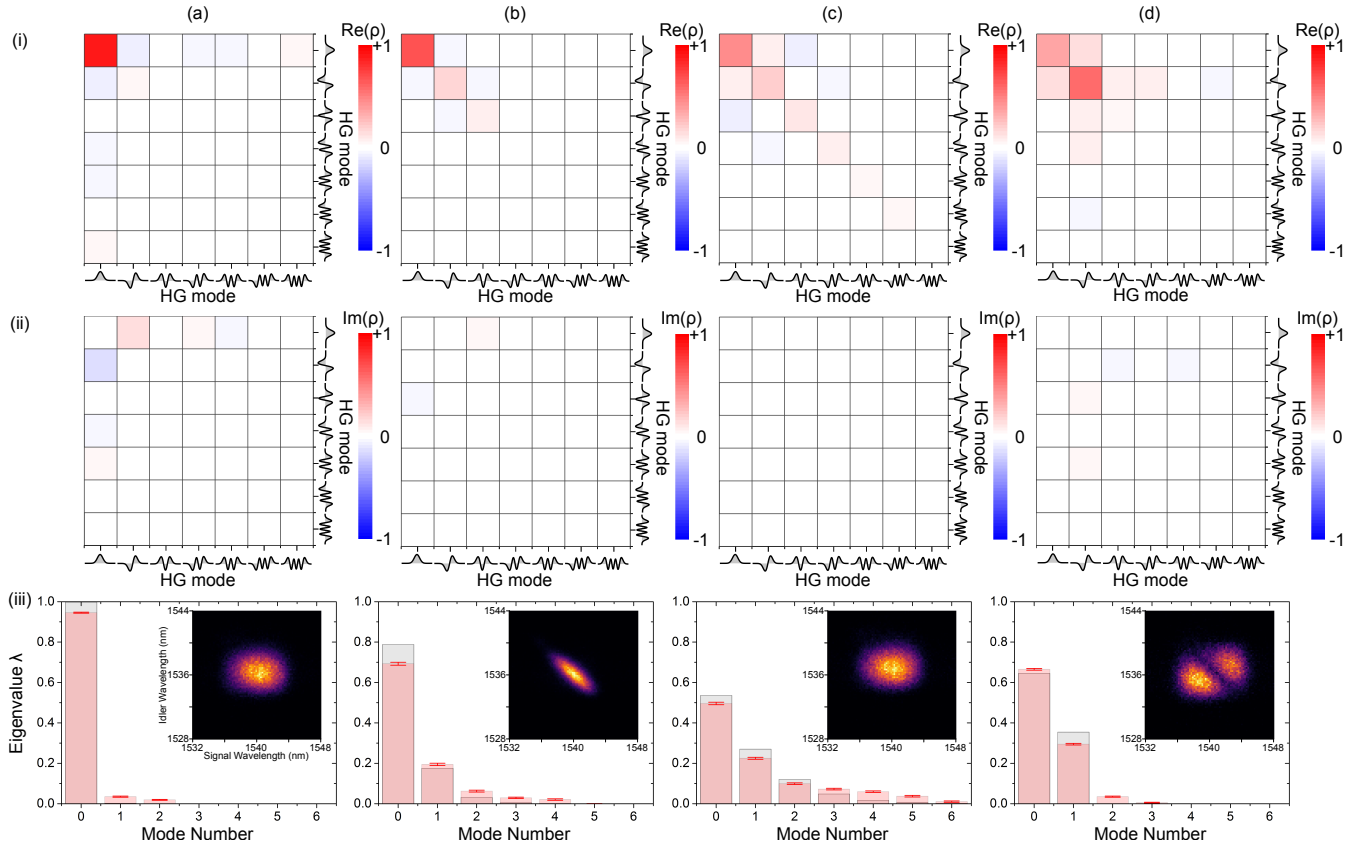

FIG. 3. **Reconstructed temporal-mode density matrices and joint spectral amplitudes.** The real (i) and imaginary (ii) parts of the reconstructed signal-photon density matrices for (a) a spectrally decorrelated PDC state, (b) an intensity-correlated state, (c) a phase-correlated state, and (d) an HG1-pumped state. The eigenvalues ($\sum \lambda = 1$) of these density matrices are shown in red in (iii), with the error bars found from Monte Carlo simulations assuming Poissonian noise. The expected one-photon density matrices from the joint spectral intensities (inset) are all diagonal with eigenvalues obtained from the singular value decomposition, as seen in gray assuming a flat phase for cases (a) and (b) and the programmed phase in (c) and (d).

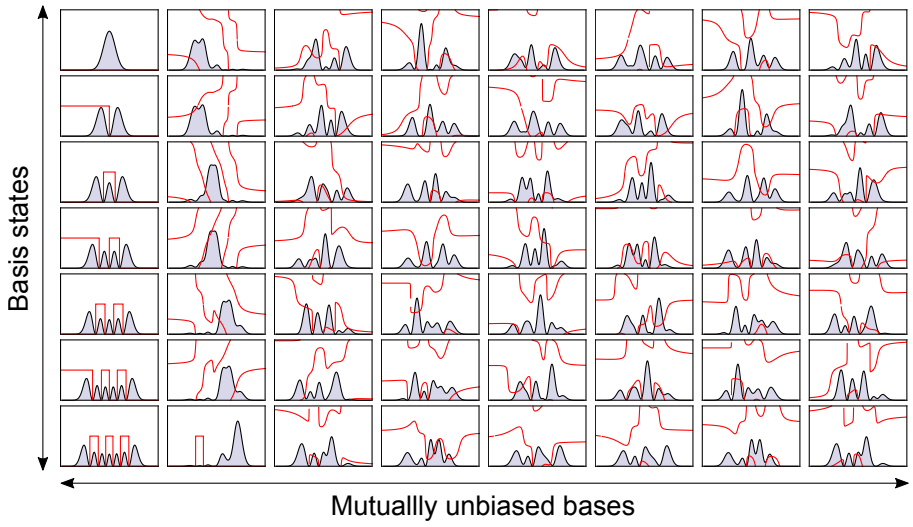

FIG. 4. **Seven-dimensional temporal-mode bases.** The spectral shapes corresponding to eight mutually unbiased seven-dimensional bases [46] as programmed for the reconstruction of Fig. 3. The black line and blue fill correspond to the intensity $|f(\omega)|^2$, and the red line corresponds to the phase on the interval $[0, 2\pi]$.

[1] J. Leach, E. Bolduc, D. J. Gauthier, and R. W. Boyd, Phys. Rev. A **85**, 060304 (2012).
[2] T. Zhong, H. Zhou, R. D. Horansky, C. Lee, V. B. Verma, A. E. Lita, A. Restelli, J. C. Bienfang, R. P. Mirin, T. Gerrits, *et al.*, New J. Phys. **17**, 022002 (2015).
[3] M. Agnew, J. Leach, M. McLaren, F. S. Roux, and R. W. Boyd, Phys. Rev. A **84**, 062101 (2011).
[4] S. Yokoyama, R. Ukai, S. C. Armstrong, C. Sornphiphatphong, T. Kaji, S. Suzuki, J.-I. Yoshikawa, H. Yonezawa, N. C. Menicucci, and A. Furusawa, Nature Photonics **7**, 982 (2013).
[5] J. Roslund, R. M. De Araujo, S. Jiang, C. Fabre, and N. Treps, Nature Photonics **8**, 109 (2014).
[6] C. Reimer, M. Kues, P. Roztocki, B. Wetzel, F. Grazioso, B. E. Little, S. T. Chu, T. Johnston, Y. Bromberg, L. Caspani, *et al.*, Science **351**, 1176 (2016).
[7] N. J. Cerf, M. Bourennane, A. Karlsson, and N. Gisin, Phys. Rev. Lett. **88**, 127902 (2002).
[8] T. Vértesi, S. Pironio, and N. Brunner, Phys. Rev. Lett. **104**, 060401 (2010).
[9] I. Herbauts, B. Blauensteiner, A. Poppe, T. Jennewein, and H. Huebel, Opt. Express **21**, 29013 (2013).
[10] W. Tittel, J. Brendel, H. Zbinden, and N. Gisin, Phys. Rev. Lett. **81**, 3563 (1998).
[11] J. Mower, Z. Zhang, P. Desjardins, C. Lee, J. H. Shapiro, and D. Englund, Phys. Rev. A **87**, 062322 (2013).
[12] J. Nunn, L. J. Wright, C. Söller, L. Zhang, I. A. Walmsley, and B. J. Smith, Opt. Express **21**, 15959 (2013).
[13] J. M. Lukens, A. Dezfooliyan, C. Langrock, M. M. Fejer, D. E. Leaird, and A. M. Weiner, Phys. Rev. Lett. **112**, 133602 (2014).
[14] B. Brecht, D. V. Reddy, C. Silberhorn, and M. G. Raymer, Phys. Rev. X **5**, 041017 (2015).
[15] S. Schwarz, B. Bessire, A. Stefanov, and Y.-C. Liang, New J. Phys. **18**, 035001 (2016).
[16] A. B. U'Ren, C. Silberhorn, R. Erdmann, K. Banaszek, W. P. Grice, I. A. Walmsley, and M. G. Raymer, Laser Physics **15**, 146 (2005).
[17] Z. Zheng and A. Weiner, Optics Lett. **25**, 984 (2000).
[18] A. Pe'er, B. Dayan, A. A. Friesem, and Y. Silberberg, Phys. Rev. Lett. **94**, 073601 (2005).
[19] A. Eckstein, B. Brecht, and C. Silberhorn, Opt. Express **19**, 13770 (2011).
[20] J. M. Donohue, M. Agnew, J. Lavoie, and K. J. Resch, Phys. Rev. Lett. **111**, 153602 (2013).
[21] D. V. Reddy, M. G. Raymer, C. J. McKinstrie, L. Mejling, and K. Rottwitt, Opt. Express **21**, 13840 (2013).
[22] M. Allgaier, V. Ansari, L. Sansoni, C. Eigner, V. Quiring, R. Ricken, G. Harder, B. Brecht, and C. Silberhorn, Nature Comm. **8**, 14288 (2017).
[23] B. Brecht, A. Eckstein, A. Christ, H. Suche, and C. Silberhorn, New J. Phys. **13**, 065029 (2011).
[24] B. Brecht, A. Eckstein, R. Ricken, V. Quiring, H. Suche, L. Sansoni, and C. Silberhorn, Phys. Rev. A **90**, 030302 (2014).
[25] A. S. Kowligy, P. Manurkar, N. V. Corzo, V. G. Velev, M. Silver, R. P. Scott, S. J. B. Yoo, P. Kumar, G. S. Kanter, and Y.-P. Huang, Opt. Express **22**, 27942 (2014).
[26] P. Manurkar, N. Jain, M. Silver, Y.-P. Huang, C. Langrock, M. M. Fejer, P. Kumar, and G. S. Kanter, Optica **3**, 1300 (2016).
[27] D. V. Reddy and M. G. Raymer, Opt. Express **25**, 12952 (2017).
[28] A. Shahverdi, Y. M. Sua, L. Tumeh, and Y.-P. Huang, Scientific Reports **7**, 6495 (2017).
[29] D. V. Reddy and M. G. Raymer, Optica **5**, 423 (2018).
[30] V. Ansari, G. Harder, M. Allgaier, B. Brecht, and C. Silberhorn, Phys. Rev. A **96**, 063817 (2017).
[31] Y.-S. Ra, C. Jacquard, A. Dufour, C. Fabre, and N. Treps, Phys. Rev. X **7**, 031012 (2017).
[32] C. Polycarpou, K. N. Cassemiro, G. Venturi, A. Zavatta, and M. Bellini, Phys. Rev. Lett. **109**, 053602 (2012).
[33] Z. Qin, A. S. Prasad, T. Brannan, A. MacRae, A. Lezama, and A. Lvovsky, Light Sci. Appl. **4**, e298 (2015).
[34] J. Tiedau, V. Shchesnovich, D. Mogilevtsev, V. Ansari, G. Harder, T. Bartley, N. Korolkova, and C. Silberhorn, New J. Phys. **20**, 033003 (2018).
[35] W. P. Grice and I. A. Walmsley, Phys. Rev. A **56**, 1627 (1997).
[36] O. Kuzucu, M. Fiorentino, M. A. Albota, F. N. C. Wong, and F. X. Kärtner, Phys. Rev. Lett. **94**, 083601 (2005).
[37] T. Gerrits, M. J. Stevens, B. Baek, B. Calkins, A. Lita, S. Glancy, E. Knill, S. W. Nam, R. P. Mirin, R. H. Hadfield, *et al.*, Opt. Express **19**, 24434 (2011).
[38] G. Harder, V. Ansari, B. Brecht, T. Dirmeier, C. Marquardt, and C. Silberhorn, Opt. Express **21**, 13975 (2013).
[39] C. K. Law, I. A. Walmsley, and J. H. Eberly, Phys. Rev. Lett. **84**, 5304 (2000).
[40] A. Christ, K. Laiho, A. Eckstein, K. N. Cassemiro, and C. Silberhorn, New J. Phys. **13**, 033027 (2011).
[41] A. M. Weiner, Rev. Sci. Instrum. **71**, 1929 (2000).
[42] A. Monmayrant, S. Weber, and B. Chatel, Journal of Physics B **43**, 103001 (2010).
[43] M. Avenhaus, A. Eckstein, P. J. Mosley, and C. Silberhorn, Opt. Lett. **34**, 2873 (2009).
[44] J. S. Pelc, L. Ma, C. Phillips, Q. Zhang, C. Langrock, O. Slattery, X. Tang, Fejer, and MM, Opt. Express **19**, 21445 (2011).
[45] W. K. Wootters and B. D. Fields, Annals of Physics **191**, 363 (1989).
[46] S. Bandyopadhyay, P. O. Boykin, V. Roychowdhury, and F. Vatan, Algorithmica **34**, 512 (2002).
[47] J. B. Altepeter, E. R. Jeffrey, and P. G. Kwiat, Advances in Atomic, Molecular, and Optical Physics **52**, 105 (2005).
[48] C. H. Bennett, H. J. Bernstein, S. Popescu, and B. Schumacher, Phys. Rev. A **53**, 2046 (1996).
[49] D. V. Reddy, M. G. Raymer, and C. J. McKinstrie, Opt. Lett. **39**, 2924 (2014).